Available online at www.sciencedirect.com
SCIENCE DIRECT®
Journal of Organometallic Chemistry 690 (2005) 3067–3079
Journal of Organometallic Chemistry
www.elsevier.com/locate/jorganchem

Ligand substitution in the mixed-metal cluster $PhCCo_2Ni(CO)_6Cp$ by 2,3-bis(diphenylphosphino)maleic anhydride (bma): An intimate picture involving the stepwise conversion of the trinuclear cluster $PhCCo_2Ni(CO)_4(\eta^2\text{-bma})Cp$ to the mononuclear compound $CpNi[PPh_2CPhC{=}C(PPh_2)C(O)OC(O)]$ ☆

Simon G. Bott [a,*], Kaiyuan Yang [b], Michael G. Richmond [b,*]

[a] Department of Chemistry, University of Houston, Houston, TX 77204, USA
[b] Department of Chemistry, University of North Texas, Denton, TX 76203, USA

Received 4 September 2004; revised 27 January 2005; accepted 28 January 2005
Available online 23 May 2005

Abstract

Heating the mixed-metal cluster $PhCCo_2Ni(CO)_6Cp$ with the diphosphine ligand 2,3-bis(diphenylphosphino)maleic anhydride (bma) in 1,2-dichloroethane proceeds by CO loss and formation of the cobalt-bridged cluster $PhCCo_2Ni(CO)_4(\eta^2\text{-bma})Cp$ (**2**). The bma ligand is fluxional in solution and is in equilibrium with the cobalt-chelated isomer, as demonstrated by VT IR and ^{31}P NMR measurements. The van't Hoff parameters ($\Delta H = 1.49 \pm 0.02$ kcal/mol; $\Delta S = 12.0 \pm 0.1$ eu) for the chelate-to-bridge equilibrium have been evaluated from IR band-shape analyses of the in-phase anhydride carbonyl stretching band over the temperature range 173–116 K. Cluster **2** readily loses CO to furnish the cluster $PhCCo_2Ni(CO)_3(\mu,\eta^2\text{-bma})Cp$ (**3**), where the $6e^-$ donor bma ligand chelates one of the cobalt centers via the phosphine groups and is tethered to the second cobalt center by the maleic anhydride π bond. Continued heating of cluster **3** is followed by the formation of $50e^-$ cluster $Co_2Ni(CO)_4Cp[\mu_2,\eta^2,\eta^1\text{-}C(Ph)C{=}C(PPh_2)C(O)OC(O)](\mu_2\text{-}PPh_2)$ (**4**), which in turn gives the mononuclear complex $CpNi[PPh_2CPhC{=}C(PPh_2)C(O)OC(O)]$ (**5**) as the end-product of the thermolysis reaction. Each of these new compounds has been isolated and their thermolysis reactivity independently examined, allowing for the unequivocal sequence associated with the decomposition of $PhCCo_2Ni(CO)_4(\eta^2\text{-bma})Cp$ to be established. Compounds **2–5** have been fully characterized in solution by IR and NMR(^1H, ^{13}C, ^{31}P) spectroscopies, and the solid-state structures of all four products have been determined by X-ray crystallography. The solution spectroscopic data of the new products are compared with the X-ray diffraction structures and the structural highlights of each compound are discussed. The coordination of the maleic anhydride π bond in $PhCCo_2Ni(CO)_3(\mu,\eta^2\text{-bma})Cp$ (**3**) provides crucial insight into one of the necessary requirements for P–C bond cleavage of the bma ligand at a tetrahedral cluster. The reactivity of the heterometallic cluster $PhCCo_2Ni(CO)_4(\eta^2\text{-bma})Cp$ is contrasted with its homometallic analogue $PhCCo_3(CO)_7(\eta^2\text{-bma})$.

Keywords: Mixed-metal clusters; P–C bond cleavage; Diphosphine fluxional behavior; VT IR

1. Introduction

The ligand substitution behavior of the homometallic clusters $RCCo_3(CO)_9$ has been thoroughly examined over the last three decades. Monodentate phosphines

☆ Dedicated to Prof. Charles U. Pittman, Jr. (aka CUP) for his work in polymer and metal cluster chemistry on the occasion of his 66th birthday.

* Corresponding authors. Tel.: +713 743 2771 (S.G. Bott), Tel.: +940 565 3548; fax: +940 564 4318 (M.G. Richmond).
E-mail addresses: sbott@uh.edu (S.G. Bott), cobalt@unt.edu (M.G. Richmond).

0022-328X/$ - see front matter © 2005 Elsevier B.V. All rights reserved.
doi:10.1016/j.jorganchem.2005.01.069

react with $RCCo_3(CO)_9$ to furnish the expected substituted derivatives $RCCo_3(CO)_{9-x}P_x$, with the degree of ligand incorporation ($x = 1$–3) strongly dependent upon the size of the incoming P ligand. In the case of multiple CO replacements, phosphine addition takes place sequentially at $Co(CO)_3$ centers leading ultimately to the trisubstituted clusters $RCCo_3(CO)_6P_3$ [1] CO substitution reactions have also been studied with bi- and tridentate phosphine ligands. This latter family of phosphine ligands gives $RCCo_3(CO)_6P_3$ compounds through the face-capping of the three cobalt atoms via axial coordination [2], with the substitution chemistry using bidentate ligands being more diverse and less predictable. There diphosphine ligands have been found to bridge adjacent cobalt centers and/or chelate to a single cobalt atom [3].

We have previously presented our findings concerning the reactivity of the redox-active diphosphine ligand 2,3-bis(diphenylphosphino)maleic anhydride (bma) with $RCCo_3(CO)_9$ (where R = Ph, Fc) to afford $RCCo_3(CO)_7(\eta^2$-bma) [4]. Of surprise to us was: (1) the coordinative flexibility exhibited by the ancillary bma ligand when tethered to the tricobalt cluster, which manifests itself in the rapid equilibration of the bridging and chelating bma isomers of $RCCo_3(CO)_7(\eta^2$-bma), and (2) the subsequent ligand/cluster fragmentation reactivity that is depicted in Scheme 1. Our findings here reveal that the nature of the capping alkylidyne moiety does indeed influence the course of ligand reactivity in these thermolysis reactions [5].

In an attempt to gain a greater understanding of the scope and generality associated with the reactivity of the bma ligand at other tetrahedrane clusters, we have explored the reaction of the mixed-metal clusters $RCCo_2Ni(CO)_6Cp$ (where R = H, Ph) with bma. Thermolysis of $HCCo_2Ni(CO)_6Cp$ with added bma produces the putative species $HCCo_2Ni(CO)_4(\eta^2$-bma)Cp, followed by bma attack at both the methylidyne cap and the CpNi center, as shown in Eq. (1). Continued heating of this product leads to P–C bond cleavage and formation of the 50e− *hypho* cluster $Co_2NiCp(CO)_4[\mu_2,\eta^2,\sigma$-$C(H)PPh_2C{=}CC(O)OC(O)](\mu_2$-$PPh_2)$ (not shown) [6].

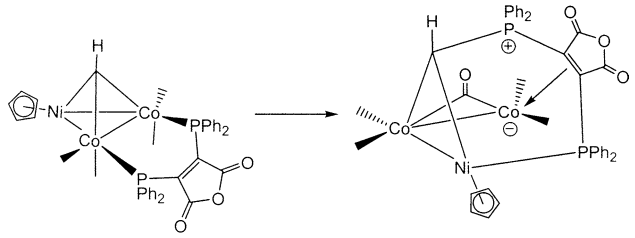

(1)

Herein, we report our results on the reaction between $PhCCo_2Ni(CO)_6Cp$ and bma, which yields $PhCCo_2Ni(CO)_4(\eta^2$-bma)Cp (**2**). The thermodynamics for chelate-to-bridge ligand isomerization in **2** have been assessed by VT IR measurements. Cluster **2** is thermally unstable and gives $PhCCo_2Ni(CO)_3(\mu,\eta^2$-bma)Cp (**3**), followed by $Co_2Ni(CO)_4Cp[\mu_2,\eta^2,\eta^1$-$C(Ph)C{=}C(PPh_2)$-$C(O)OC(O)](\mu_2$-$PPh_2)$ (**4**). Continued heating of cluster **4** is accompanied by cluster fragmentation and formation of mononuclear nickel complex $CpNi[PPh_2$-$CPhC{=}C(PPh_2)C(O)OC(O)]$ (**5**) as the end-product. Clusters **2**–**5** have been isolated and fully characterized in solution by standard spectroscopic methods and the solid-state structures of all four products have all been determined by X-ray crystallography. The reactivity of the heterometallic cluster $PhCCo_2Ni(CO)_4(\eta^2$-bma)Cp is discussed relative to its homometallic counterpart $PhCCo_3(CO)_7(\eta^2$-bma).

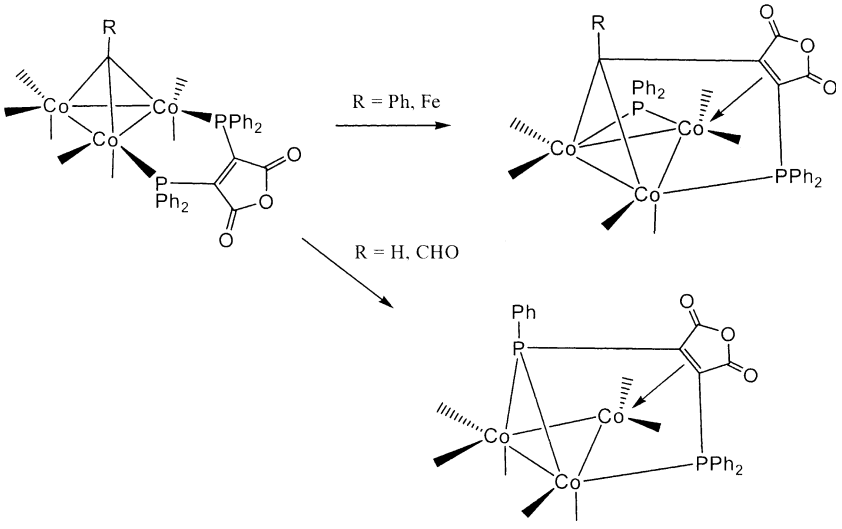

Scheme 1.

2. Experimental

2.1. General methods

The bma ligand was synthesized from 2,3-dichloromaleic anhydride, which was purchased from Aldrich Chemical Co. and used as received, and Ph_2PTMS [7]. The starting cluster $PhCCo_2Ni(CO)_6Cp$ was prepared from $PhCCo_3(CO)_9$ [8] and nickelocene [9] according to the general procedure of Vahrenkamp [10]. All reaction and NMR solvents were distilled under argon from a suitable drying agent and stored in Schlenk storage vessels [11]. The combustion analyses were performed by Altantic Microlab, Norcross, GA.

Routine solution infrared spectra were recorded on a Nicolet 20 SXB FT-IR spectrometer in amalgamated 0.1 mm NaCl cells, using PC control and OMNIC software. The VT IR spectra were recorded on the above spectrometer with a Specac Model P/N 21.000 IR cell equipped with inner and outer CaF_2 windows and modified for flow sampling conditions. The coolant employed in the VT IR studies was either liquid nitrogen (<143 K) or a pentane/liquid nitrogen slush (173–143 K). The reported cell temperatures, taken to be accurate to ±2 °C, were determined with a Cu-constantan thermocouple. The ^1H NMR spectra were recorded at 200 MHz on a Varian Gemini-200 spectrometer, and the ^{13}C and ^{31}P NMR spectra were recorded at 75 and 121 MHz, respectively, on a Varian 300-VXR spectrometer in the proton decoupled mode. The reported ^{31}P chemical shifts are referenced to external H_3PO_4 (85%), taken to have $\delta = 0.0$.

2.2. Synthesis of $PhCCo_2Ni(CO)_4(\eta^2$-bma)Cp (2) from $PhCCo_2Ni(CO)_6Cp$ (1)

To 0.30 g (0.60 mmol) of $PhCCo_2Ni(CO)_6Cp$ and 0.30 g (0.64 mmol) of bma in a large Schlenk tube was added 30 mL of 1,2-dichloroethane (DCE) by syringe, after which the vessel was sealed and heated at 75–80 °C for ca. 0.5 h. Yields of $PhCCo_2Ni(CO)_4(\eta^2$-bma)Cp were maximized when the reaction solution was monitored by TLC analysis and heating terminated when clusters **3** and **4** and decomposition material at the origin was observed. Upon such time the solvent was removed under vacuum and the product cluster was purified by flash column chromatography over silica gel using a 1:1 mixture of CH_2Cl_2/petroleum ether as the eluent. Recrystallization of $PhCCo_2Ni(CO)_4(\eta^2$-bma)Cp from a CH_2Cl_2 solution that had been layered with hexane afforded the analytical sample and single crystals of **2** suitable for X-ray diffraction analysis. Yield of green $PhCCo_2Ni(CO)_4(\eta^2$-bma)Cp: 0.35 g (67%). IR (CH_2Cl_2; 298 K): ν(CO) 2012 (s), 1989 (vs), 1971 (s), 1821 (w, symm anhydride carbonyl), 1767 (m, antisymm anhydride carbonyl) cm^{-1}. ^1H NMR ($CDCl_3$; 298 K): δ 5.15 (s, Cp), 6.75–7.75 (m, phenyls). ^{13}C (CH_2Cl_2; 183 K) δ 201.03 (chelating isomer), 203.41 (s, 2C, bridging isomer), 209.75 (2C, bridging isomer). ^{31}P NMR ($CDCl_3$; 298K): δ 24.24 (b, bridging isomer); (THF; 173 K) δ 25.48 (s, bridging isomer), 51.45 (s, chelating isomer), 59.50 (s, chelating isomer). Anal. Calc. (found) for $C_{44}H_{30}Co_2NiO_7P_2$: C, 58.10 (57.89); H, 3.32 (3.38).

2.3. Thermolysis of $PhCCo_2Ni(CO)_4(\eta^2$-bma)Cp (2) to give $PhCCo_2Ni(CO)_3(\mu,\eta^2$-bma)Cp (3) and $Co_2Ni(CO)_4Cp[\mu_2,\eta^2,\eta^1$-C(Ph)C=C($PPh_2$)C(O)OC(O)] ($\mu_2$-$PPh_2$) (4)

To a Schlenk tube containing 0.30 g (0.33 mmol) of $PhCCo_2Ni(CO)_4(\eta^2$-bma)Cp was added 25 mL of DCE under argon flush. The solution was then heated at reflux for 3.0 h, at which time maximum conversion to clusters **3** and **4** was found by TLC analysis. The DCE solvent was removed and the components in the reaction mixture separated by column chromatography over silica gel using CH_2Cl_2 as the eluent. The first green band isolated from the column belonged to **2**, followed by a second green band corresponding to $PhCCo_2Ni(CO)_3(\mu,\eta^2$-bma)Cp (**3**), and finally a brown band due to $Co_2Ni(CO)_4Cp[\mu_2,\eta^2,\eta^1$-C(Ph)C=C($PPh_2$)C(O)OC(O)] ($\mu_2$-$PPh_2$) (**4**). Cluster **3** was recrystallized from a CH_2Cl_2 solution that had been layered with hexane, while cluster **4** was recrystallized from a benzene solution that had been layered with hexane. These recrystallizations furnished X-ray quality crystals and the samples for combustion analysis. Yield of $PhCCo_2Ni(CO)_3(\mu,\eta^2$-bma)Cp: 65 mg (21%). IR (CH_2Cl_2; 298 K): ν(CO) 2006 (s), 1954 (vs), 1912 (s, semibridging CO), 1789 (m, symm anhydride carbonyl), 1740 (m, antisymm anhydride carbonyl) cm^{-1}. ^1H NMR ($CDCl_3$; 298 K): δ 4.69 (s, Cp), 6.80–9.70 (m, phenyls). ^{13}C (THF; 223 K) δ 201.31 (1C) 209.46 (1C), 223.79 (1C, semibridging CO). ^{31}P NMR (THF; 178 K): δ 25.30 (s, b), 29.57 (s, b). Anal. Calc. (found) for $C_{43}H_{30}Co_2NiO_6P_2$: C, 58.59 (58.32); H, 3.45 (3.56). Yield of $Co_2Ni(CO)_4Cp[\mu_2,\eta^2,\eta^1$-C(Ph)C=C($PPh_2$)C(O)OC(O)]($\mu_2$-$PPh_2$): 75 mg (25%). IR ($CH_2Cl_2$; 298 K): ν(CO) 2032 (s), 2000 (vs), 1985 (m), 1962 (m) 1798 (m, symm anhydride carbonyl), 1739 (m, antisymm anhydride carbonyl) cm^{-1}. ^1H NMR ($CDCl_3$; 298 K): δ 4.83 (s, Cp), 7.00–8.50 (m, phenyls). ^{13}C (THF; 223 K) δ 201.74 (s, b) 206.10 (s, b), 206.55 (s, b) 209.67 (s, b). ^{31}P NMR (THF; 178 K): δ 63.88 (Ni–P), 170.94 (s, phosphido). Anal. Calc. (found) for $C_{44}H_{30}Co_2NiO_7P_2 \cdot C_6H_6$: C, 60.82 (60.53); H, 3.67 (3.70).

2.4. Thermolysis of $Co_2Ni(CO)_4Cp[\mu_2,\eta^2,\eta^1$-C(Ph)C=C($PPh_2$)C(O)OC(O)]($\mu_2$-$PPh_2$) to CpNi[$PPh_2$CPhC=C($PPh_2$)C(O)OC(O)] (5)

The thermolysis was carried out with 0.30 g (0.33 mmol) of cluster **4** in 25 mL of DCE. The solution

was heated at reflux in a Schlenk vessel under argon for ca. 2 days until only a trace of starting cluster remained, as determined by TLC analysis. The DCE solvent was removed under vacuum and the sole observable product of the reaction was isolated by chromatography over silica gel using a 9:1 mixture of CH_2Cl_2/acetone. The resulting CpNi[$PPh_2CPhC{=}C(PPh_2)(O)OC(O)$] that was obtained was recrystallized from CH_2Cl_2 and hexane by allowing the former solvent to evaporate slowly under argon protection. Yield of black **5**: 30 mg (13%). IR (CH_2Cl_2): ν(CO) 1746 (m, symm anhydride carbonyl), 1714 (s, antisymm anhydride carbonyl) cm^{-1}. ^1H NMR ($CDCl_3$; 298 K): δ 4.92 (s, Cp), 6.70–7.35 (m, phenyls). ^{13}C NMR ($CDCl_3$; 298 K): δ 94.75 (Cp). ^{31}P NMR ($CDCl_3$, 298 K): δ 12.22 (d, $J_{P-P} = 76$ Hz), 42.07 (d, $J_{P-P} = 76$ Hz). Anal. Calc. (found) for $C_{40}H_{30}NiO_3P_2$: C, 70.66 (70.08); H, 4.43 (4.53).

2.5. X-ray crystallography

Table 2 contains the X-ray data and processing parameters for the structures **2**–**5**. Selected crystals of the four compounds for X-ray diffraction analysis were grown as described above and were each sealed inside a Lindemann capillary, followed by mounting on an Enraf-Nonius CAD-4 diffractometer. After the cell constants were obtained for all four samples, intensity data in the range of $2° \leqslant 2\theta \leqslant 32°$ (**2**), $2° \leqslant 2\theta \leqslant 25°$ (**3**), $2° \leqslant 2\theta \leqslant 28°$ (**4**), and $2° \leqslant 2\theta \leqslant 26°$ (**5**) were collected at 298 K and were corrected for Lorentz, polarization, and absorption (DIFABS). All four structures were solved by using SHELX-86. All non-hydrogen atoms were located with difference Fourier maps and full-matrix least-squares refinement and were refined anisotropically in cluster **2**. The data reduction in **3** proceeded similarly with the Ni, Co, P, O, and Cp groups being refined anisotropically, and with the exception of the phenyl carbon atoms in cluster **4**, all other non-hydrogen atoms were refined anisotropically. In the case of the compound **5** only the Ni and P atoms were refined anisotropically. Refinement on **2** converged at $R = 0.0318$ and $R_w = 0.0334$ for 3619 unique reflections with $I > 3\sigma(I)$, while for **3** refinement converged at $R = 0.0426$ and $R_w = 0.0459$ for 2551 unique reflections with $I > 3\sigma(I)$. The refinement for **4** and **5** afforded convergence values of $R = 0.0466$ and $R_w = 0.0507$ for 2902 unique reflections with $I > 3\sigma(I)$ and $R = 0.0934$ and $R_w = 0.1094$ for 2676 unique reflections with $I > 3\sigma(I)$, respectively.

2.6. Thermodynamic assessment of the equilibrium between the bridging and chelating isomers of $PhCCo_2Ni(CO)_4(\eta^2\text{-bma})Cp$

2-MeTHF solutions of $PhCCo_2Ni(CO)_4(\eta^2$-bma)Cp (ca. 7.0×10^{-3} M) were used to measure the amount of bridging and chelating isomer in solution over the temperature range of 173–116 K. The temperature-dependent behavior associated with the in-phase anhydride carbonyl stretching band of each isomer was analyzed by VT IR spectroscopy, with the area of each band quantified by band-shape analysis using the commercially available program Peakfit and where the area under each carbonyl absorption was assumed to be proportional the relative amount of each isomer. All spectra were subjected to base-line correction and were successfully fitted by using Gaussian band shapes. The thermodynamic parameters for the chelate $\rightleftharpoons$ bridge exchange were obtained from a plot of ln K_{eq} vs. T^{-1}, from which the slope and intercept furnished the ΔH and ΔS, respectively. The error limits for the thermodynamic data were calculated by using the available least-squares regression program and do not reflect uncertainties in sample preparation, band-area intensities, or temperature control but rather the deviation of the data points about the least-squares line [12].

3. Results and discussion

3.1. Reaction of $PhCCo_2Ni(CO)_6Cp$ with bma, spectroscopic evidence for diphosphine isomerization, and X-ray diffraction structure of $PhCCo_2Ni(CO)_4(\eta^2\text{-bma})Cp$

Heating an equimolar mixture of $PhCCo_2Ni(CO)_6Cp$ (**1**) with the diphosphine ligand bma in DCE at 75–80 °C promotes the loss of CO and formation of the substituted cluster $PhCCo_2Ni(CO)_4(\eta^2$-bma)Cp (**2**) without the presence of other products, provided the reaction time is kept short. Maximum yields of **2** were realized when the reaction was monitored by IR or TLC analysis and terminating the reaction at the first sign of by-products. Cluster **2** was isolated by chromatography over silica gel as a mildly air-sensitive green solid. The reaction between cluster **1** and bma is shown in Eq. (2).

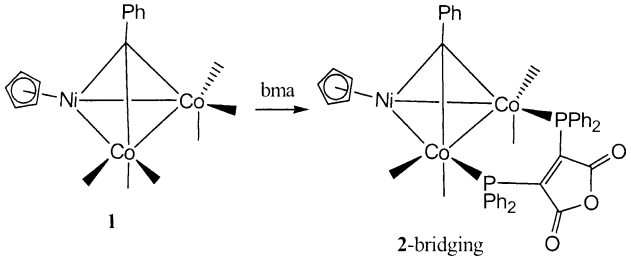

(2)

The room temperature ^{31}P NMR spectrum of **2** revealed the presence of a broad resonance at ca. δ 24 suggesting the presence of a bridging bma ligand [13]. Since it was not immediately clear whether the broadened resonance was due to scalar coupling between the ^{31}P and ^{59}Co nuclei or dynamic isomerism of the bma about the cluster polyhedron [14], we examined the ^{31}P

NMR spectrum at reduced temperature. The resonance at δ 24 sharpened considerably as the temperature was dropped to 248 K and was accompanied by the appearance of two very weak resonances at ca. δ 50 and 60. Further cooling to 173 K, the lowest attainable temperature on our spectrometer, led to an increase in the intensity of the latter two low-field resonances at the expense of the bridging resonance at δ 25.48, and in keeping with the bma isomerization behavior found in $PhCCo_3(CO)_7(\eta^2$-bma), the two equal intensity resonances at δ 51.45 and 59.50 are assigned to the chelating isomer of $PhCCo_2Ni(CO)_4(\eta^2$-bma)Cp. Integration of the ^{31}P NMR data at 173 K gives a K_{eq} of 5.7 in favor of the bma-bridged cluster **2**. The equilibrium constant calculated for **2** is identical to that reported by us for $PhCCo_3(CO)_7(\eta^2$-bma), [4a] where the bma-bridged cluster was found to be favored under the same conditions. While this may appear fortuitous, we would not expect the dynamics for bma ligand fluxionality to be substantially different between $PhCCo_2Ni(CO)_4(\eta^2$-bma)Cp and $PhCCo_3(CO)_7(\eta^2$-bma) given the structural/electronic similarities of the cobalt centers that participate in the isomerization sequence. The isomeric forms of $PhCCo_2Ni(CO)_4(\eta^2$-bma)Cp that contribute to this equilibrium are shown in the top portion of Scheme 2.

The ^{13}C NMR spectrum of ^{13}CO enriched **2** exhibited two broad terminal carbonyl resonances at δ 203 and 209 with an integral ratio of 1:1 at 298 K. These groups are readily assigned to the pairwise equivalent axial and equatorial Co–CO groups in the bma-bridged cluster possessing C_s symmetry. Recording the same sample at

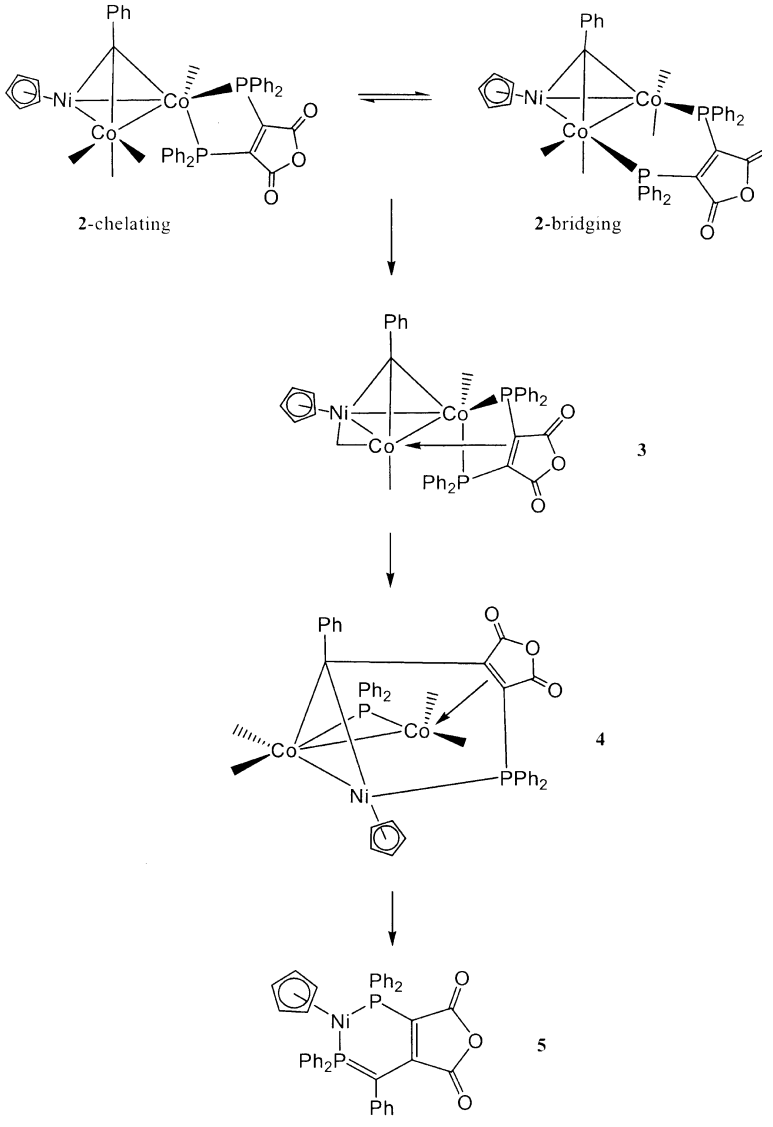

35

Scheme 2.

183 K led to a sharpening of the two CO groups of the bridged isomer and produced a small, broad carbonyl signal at δ 201. This behavior is fully reversible and the chemical shift at δ 201 is ascribed to the three terminally bound Co–CO groups in the chelating isomer of **2**, on the basis of chemical shift arguments and the VT ^{13}C NMR data reported for $PhCCo_3(CO)_7(\eta^2$-bma). Not observed in the chelating isomer of **2** is the expected low-field resonance for the lone CO group center that is bound at the phosphine-tethered cobalt center. The absence of this CO group may be due to the rapid intramolecular scrambling of all the CO ligands in the chelating isomer or ^{59}Co quadrupolar broadening. In either case spectral observation would be problematic.

Additional proof for the isomerization of the bma ligand in $PhCCo_2Ni(CO)_4(\eta^2$-bma)Cp and thermodynamic assessment of the chelate ⇄ bridge equilibrium were provided by VT FT-IR measurements. The room temperature IR spectrum of **2** in CH_2Cl_2 solvent displays three prominent terminal ν(CO) bands at 2012, 1989, and 1971 cm^{-1}, along with two weaker ν(CO) bands at 1821 and 1767 belonging to the vibrationally coupled anhydride moiety [15]. Recording the same spectrum right above the freezing point of CH_2Cl_2 revealed additional small but observable anhydride carbonyl stretching bands. Since the chelating isomer is favored at low temperature and that we were temperature limited in CH_2Cl_2, we employed 2-MeTHF as a solvent. The IR spectra of **2** in 2-MeTHF at temperatures <173 K showed a sharpening of the terminal CO groups associated with the two cobalt atoms, but the three observed carbonyl bands exhibited insufficient resolution to make them of any use in the study of the two isomers. However, the two ν(CO) bands belonging to the anhydride ring did provide the means by which this equilibrium could be studied. Fig. 1 shows the IR spectra for the anhydride ν(CO) bands of cluster **2** recorded at 173 and 116 K. At 173 K in 2-MeTHF the higher energy in-phase ν(CO) band at 1821 cm^{-1} of the ligand-bridged isomer is accompanied by a weaker intensity shoulder at 1830 cm^{-1}. This doubling of ν(CO) bands was also found with the lower energy antisymmetric ν(CO) band; here ν(CO) bands at 1761 (bridge) and 1770 (chelate) cm^{-1} were recorded. As the temperature was progressively lowered, the bands at 1821 and 1761 cm^{-1} decreased in intensity as the other two ν(CO) bands of the chelating isomer increased. The changes were reversible, as confirmed by several independent experiments and repeated cycling of the temperature over the range of 173–116 K.

The IR spectra were subjected to band-area measurements in order to determine the area under each in-phase carbonyl stretching band [16]. Table 1 lists the K_{eq} values for the equilibrium involving chelate-to-bridge exchange, from which the van't Hoff plot that accompanies Fig. 1 afforded values of 1.49 ± 0.02 kcal/mol for ΔH and 12.0 ± 0.1 eu for ΔS. The opposing

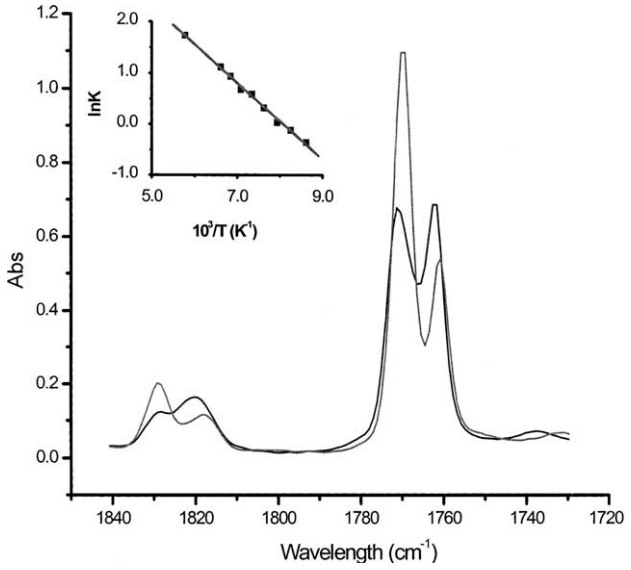

Fig. 1. VT FT-IR spectra of $PhCCo_2Ni(CO)_4(\eta^2$-bma)Cp (**2**) in the anhydride carbonyl region at 173 (black) and 116 K (red) in 2-MeTHF solvent, with inclusion of the van't Hoff plot as an inset.

Table 1
Equilibrium data for the conversion of chelating **2** into bridging **2**[a]

$10^3/T$, K^{-1}	Chelating (%)	Bridging (%)	ln K_{eq}[b]
5.78	15.0	85.0	1.73
6.62	24.3	74.7	1.12
6.85	28.0	72.0	0.94
7.09	33.6	66.4	0.68
7.35	35.7	64.3	0.59
7.63	42.0	58.0	0.32
7.94	49.2	50.8	0.032
8.26	53.0	47.0	−0.12
8.62	59.0	41.0	−0.36

ΔH = 1.49 ± 0.02 kcal/mol; ΔS = 12.0 ± 0.1 eu.

[a] From 7.0×10^{-3} M $PhCCo_2Ni(CO)_4(\eta^2$-bma)Cp in 2-MeTHF by following the changes in the area of the in-phase carbonyl stretching bands at 1821 and 1830 cm^{-1}.

[b] Defined as the area of [bridged isomer]/[chelated isomer].

enthalpic and entropic contributions reveal that above ca. 125 K the predominant isomer in solution will correspond to the cluster with a bridging bma ligand. Other than our original study on $PhCCo_3(CO)_7(\eta^2$-bma) where bma ligand fluxionality was verified by ^{31}P NMR spectroscopy, our current studies have provided additional evidence for the isomerization of the ancillary bma ligand through both ^{31}P and IR spectroscopies. To our knowledge, the only other report for related bidentate ligand fluxionality derives from the demonstrated racemization reactivity involving the ancillary ligands in the tetrahedrane clusters $Me_2CHO_2CCCo_3(CO)_7$(L–L) (where L–L = dppe, arphos). In the case of the arphos ligand ($Ph_2PCH_2CH_2$ $AsPh_2$), it has been suggested that the observed racemization results from the migration of the arsine moiety between the cobalt centers [17], with the ancillary ligand maintaining its

Table 2
X-ray crystallographic data and processing parameters for the compounds **2**–**5**

Compound	**2**	**3**	**4**	**5**
CCDC entry no.	244754	244755	244756	245326
Crystal system	Monoclinic	Monoclinic	Monoclinic	Triclinic
Space group	$P2_1/n$	$P2_1/c$	$P2_1/n$	$P\bar{1}$
Unit cell dimensions				
a (Å)	12.3179(9)	14.188(2)	13.618(1)	14.633(7)
b (Å)	16.382(1)	14.344(1)	22.736(3)	14.826(8)
c (Å)	19.662(1)	19.547(3)	14.5181(9)	17.798(2)
α (°)				69.04(3)
β (°)	94.461(6)	109.54(1)	100.886(8)	68.97(3)
γ (°)				65.29(5)
V (Å^{-3})	3966.3(5)	3749.0(8)	4414.2(6)	3174(3)
Mol. formula	$C_{44}H_{30}Co_2NiO_7P_2$	$C_{43}H_{30}Co_2NiO_6P_2$	$C_{50}H_{36}Co_2NiO_7P_2$	$C_{40}H_{30}NiO_2P_2$
F_w	909.25	881.24	987.36	679.34
Formula units per cell (Z)	4	4	4	4
D_{calc} (g/cm^3)	1.523	1.561	1.486	1.421
λ (Mo Kα) (Å)	0.71073	0.71073	0.71073	0.71073
Absorption coeff. (cm^{-1})	14.26	15.05	12.88	7.50
R_{merge}	0.018	0.031	0.026	–
Abs. corr. factor	0.84–1.19	0.80–1.14	0.89–1.06	0.68/1.26
Total reflections	5310	5036	5840	7193
Independent reflections	3619	2551	2902	2676
Data/res/parameters	3619/0/505	2551/0/312	2902/0/387	2676/0/389
R	0.0318	0.0426	0.0466	0.0934
R_w	0.0334	0.0459	0.0507	0.1094
GOF on F_2	0.93	1.02	1.01	1.08
Weights	$[0.04F^2 + (\sigma F)^2]^{-1}$	$[0.04F^2 + (\sigma F)^2]^{-1}$	$[0.04F^2 + (\sigma F)^2]^{-1}$	$[0.04F^2 + (\sigma F)^2]^{-1}$

bridging coordination mode upon completion of the equilibration sequence [18,19].

The molecular structure of **2** was established by X-ray crystallography and with it the bridging of the two cobalt centers by the bma ligand. Fig. 2 shows the the ORTEP diagram of $PhCCo_2Ni(CO)_4(\eta^2$-bma)Cp, with selected bond distances and angles reported in Table 3. The overall structure of **2** is unchanged from the parent cluster **1**, insomuch that it contains 48 valence electrons and a *nido* $Co_2Ni(\mu_3$-C) core [20]. Cluster **2**, to our knowledge, represents only the second structurally characterized $PhCCo_2Ni(CO)_4$ (P–P)Cp cluster to date [21]. The Co(1)–Co(2), Ni–Co(1), and Ni–Co(2) bond distances of 2.4639(9), 2.3742(9), and 2.3811(9) Å, respectively, are unremarkable in comparison to related Co_2Ni and $CoNi_2$ clusters [22], and are consistent with metal–metal single-bond distances. The C(11)–C(15) π bond of the maleic anhydride residue reveals a distance of 1.353(6) Å that is in agreement with the C=C bond distance of simple alkenes [23]. The two phosphorus groups are nearly *trans* to the CpNi moiety given the bond angles of 156.87(5)° and 150.57(5)° found for the Ni–Co(2)–P(2) and Ni–Co(1)–P(1) linkages, respectively. The plane defined by the core atoms of the maleic anhydride ring is distinctly tipped out and away from the plane of the Co_2Ni atoms based on the observed dihedral angle of ca. 62°, which in turn causes the ancillary phenyl rings comprised by the atoms C(111)–C(116) and C(211)–C(216) to adopt an essentially coplanar arrangement given the observed dihedral angle of ca. 5°.

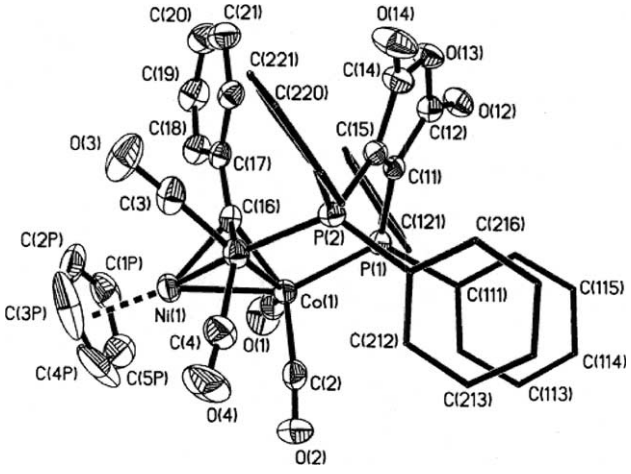

Fig. 2. ORTEP drawing of $PhCCo_2Ni(CO)_4(\eta^2$-bma)Cp (**2**) showing the thermal ellipsoids at the 50% probability level.

3.2. Thermolysis of $PhCCo_2Ni(CO)_4(\eta^2$-bma)Cp to give $PhCCo_2Ni(CO)_3(\mu,\eta^2$-bma)Cp and $Co_2Ni(CO)_4Cp$-$[\mu_2,\eta^2,\eta^1$-C(Ph)C=C(PPh_2)C(O)OC(O)](μ_2-PPh_2), and X-ray diffraction evidence for bma π-bond coordination and metal core expansion

Thermolysis of $PhCCo_2Ni(CO)_4(\eta^2$-bma)Cp in refluxing DCE furnishes the new clusters $PhCCo_2Ni(CO)_3(\mu,\eta^2$-bma)Cp (**3**) and $Co_2Ni(CO)_4Cp[\mu_2,\eta^2,\eta^1$-C(Ph)C=C($PPh_2$)C(O)OC(O)]($\mu_2$-$PPh_2$) (**4**) in nearly equal amounts during the early stages of the reaction

Table 3
Selected bond distances (Å) and angles (°) in the compounds **2**–**5**[a]

$PhCCo_2Ni(CO)_4(\eta^2$-bma)Cp (**2**)			
Bond distances			
Ni–Co(1)	2.3742(9)	Ni–Co(2)	2.3811(9)
Ni–Cp(centroid)	1.748(8)	Co(1)–Co(2)	2.4639(9)
Co(1)–P(1)	2.211(1)	Co(1)–C(1)	1.769(5)
Co(1)–C(2)	1.792(5)	Co(2)–P(2)	2.192(1)
Co(2)–C(3)	1.753(5)	Co(2)–C(4)	1.802(6)
C(11)–C(12)	1.496(6)	C(11)–C(15)	1.353(6)
C(14)–C(15)	1.490(7)		
Bond angles			
Ni–Co(1)–P(1)	150.57(5)	Co(2)–Co(1)–P(1)	106.68(4)
P(1)–Co(1)–C(1)	96.4(2)	P(1)–Co(1)–C(2)	111.8(2)
C(1)–Co(1)–C(2)	99.4(2)	Ni–Co(2)–P(2)	156.87(5)
Co(1)–Co(2)–P(2)	99.61(4)	P(2)–Co(2)–C(3)	102.1(2)
P(2)–Co(2)–C(4)	99.4(2)	C(3)–Co(2)–C(3)	102.6(3)
Co(1)–P(1)–C(11)	115.5(1)	Co(2)–P(2)–C(15)	111.5(1)
Co(1)–C(1)–O(1)	176.7(5)	Co(1)–C(2)–O(2)	173.6(5)
Co(2)–C(3)–O(3)	174.2(5)	Co(2)–C(4)–O(4)	176.9(5)
$PhCCo_2Ni(CO)_3(\mu,\eta^2$-bma)Cp (**3**)			
Bond distances			
Ni–Co(1)	2.491(2)	Ni–Co(2)	2.420(2)
Ni–C(2)	2.114(7)	Ni–Cp(centroid)	1.737(9)
Co(1)–Co(2)	2.405(1)	Co(1)–P(1)	2.178(3)
Co(1)–P(2)	2.249(2)	Co(1)–C(1)	1.760(8)
Co(2)–C(2)	1.821(9)	Co(2)–C(3)	1.78(1)
Co(2)–C(11)	2.025(9)	Co(2)–C(15)	2.064(8)
C(11)–C(12)	1.50(1)	C(11)–C(15)	1.43(1)
C(14)–C(15)	1.447(9)		
Bond angles			
Co(1)–Ni–C(2)	92.8(2)	Co(2)–Ni–C(2)	46.7(3)
Ni–Co(1)–P(1)	132.61(8)	Ni–Co(1)–P(2)	99.76(7)
Ni–Co(1)–C(1)	110.9(3)	Co(2)–Co(1)–P(1)	77.70(7)
Co(2)–Co(1)–P(2)	76.96(7)	Co(2)–Co(1)–C(1)	167.9(3)
P(1)–Co(1)–P(2)	87.83(9)	P(1)–Co(1)–C(1)	108.5(3)
P(2)–Co(1)–C(1)	113.1(3)	Ni–Co(2)–C(2)	57.7(2)
Ni–Co(2)–C(3)	115.4(3)	Ni–Co(2)–C(11)	141.2(2)
Ni–Co(2)–C(15)	123.2(2)	Co(1)–Co(2)–C(2)	103.8(3)
Co(1)–Co(2)–C(3)	150.4(3)	Co(1)–Co(2)–C(11)	79.2(2)
Co(1)–Co(2)–C(15)	81.3(2)	C(2)–Co(2)–C(3)	97.3(4)
C(2)–Co(2)–C(11)	136.2(4)	C(2)–Co(2)–C(15)	95.7(4)
C(3)–Co(2)–C(11)	99.6(4)	C(3)–Co(2)–C(15)	117.2(4)
C(11)–Co(2)–C(15)	40.9(3)	Co(1)–C(1)–O(1)	178(1)
Ni–C(2)–Co(2)	75.5(3)	Ni–C(2)–O(2)	128.0(7)
Co(2)–C(2)–O(2)	156.3(7)	Co(2)–C(3)–O(3)	179(1)
$Co_2Ni(CO)_4Cp[\mu_2,\eta^2,\eta^1$-C(Ph)C=C($PPh_2$)C(O)OC(O)]($\mu_2$-$PPh_2$) (**4**)			
Bond distances			
Ni–Co(1)	2.434(2)	Ni–P(1)	2.165(3)
Ni–Cp(centroid)	1.76(1)	Ni–C(16)	2.018(8)
Co(1)–Co(2)	2.595(2)	Co(1)–P(2)	2.164(3)
Co(1)–C(1)	1.76(1)	Co(1)–C(2)	1.806(9)
Co(1)–C(16)	1.946(8)	Co(2)–P(2)	2.167(3)
Co(2)–C(3)	1.78(1)	Co(2)–C(4)	1.80(1)
Co(2)–C(11)	2.019(8)	Co(2)–C(15)	2.067(8)
C(11)–C(12)	1.46(1)	C(11)–C(15)	1.45(1)
C(14)–C(15)	1.45(1)		
Bond angles			
Co(1)–Ni–P(1)	96.89(8)	P(1)–Ni–C(16)	90.1(3)
Ni–Co(1)–P(2)	150.87(9)	Ni–Co(1)–C(1)	105.3(3)
Ni–Co(1)–C(2)	93.5(3)	Ni–Co(1)–C(16)	53.5(2)
Co(2)–Co(1)–P(2)	53.25(8)	Co(2)–Co(1)–C(1)	149.1(3)

Table 3 (*continued*)

Co(2)–Co(1)–C(2)	99.2(3)	P(2)–Co(1)–C(1)	98.7(3)
P(2)–Co(1)–C(2)	99.3(3)	P(2)–Co(1)–C(16)	105.1(3)
C(1)–Co(1)–C(2)	98.1(4)	Co(1)–Co(2)–P(2)	53.13(7)
Co(1)–Co(2)–C(3)	146.5(3)	Co(1)–Co(2)–C(4)	98.2(3)
Co(1)–Co(2)–C(11)	91.7(2)	Co(1)–Co(2)–C(15)	71.9(2)
P(2)–Co(2)–C(3)	98.59(3)	P(2)–Co(2)–C(4)	96.2(3)
P(2)–Co(2)–C(11)	140.8(3)	P(2)–Co(2)–C(15)	104.0(3)
C(3)–Co(2)–C(4)	102.7(4)	C(3)–Co(2)–C(11)	106.8(4)
C(3)–Co(2)–C(15)	103.8(4)	C(4)–Co(2)–C(11)	106.6(4)
C(4)–Co(2)–C(15)	143.7(4)	C(11)–Co(2)–C(15)	41.5(4)
Co(1)–C(1)–O(1)	173.3(8)	Co(1)–C(2)–O(2)	175(1)
Co(2)–C(3)–O(3)	177.2(9)	Co(2)–C(4)–O(4)	177.2(9)
$CpNi[PPh_2CPhC{=}C(PPh_2)C(O)OC(O)]$ (**5**)			
Bond distances			
Molecule A		molecule B	
Ni(1)–P(1)	2.152(9)	Ni(2)–P(3)	2.147(9)
Ni(1)–P(2)	2.137(6)	Ni(2)–P(4)	2.160
Ni(1)–Cp(centroid)	1.72(1)	Ni(2)–Cp(centroid)	1.74(2)
P(1)–C(11)	1.78(2)	P(3)–(31)	1.75(2)
P(2)–C(16)	1.79(2)	P(4)–C(36)	1.79(2)
C(11)–C(12)	1.38(3)	C(31)–C(32)	1.42(3)
C(11)–C(15)	1.45(3)	C(31)–C(35)	1.38(3)
C(14)–C(15)	1.45(3)	C(34)–C(35)	1.51(3)
Bond angles			
P(1)–Ni(1)–P(2)	93.8(3)	P(3)–Ni(2)–P(4)	93.4(3)
Ni(1)–P(1)–C(11)	112.8(9)	Ni(2)–P(3)–C(31)	112(1)
Ni(1)–P(2)–C(16)	116.0(7)	Ni(2)–P(4)–C(36)	117.7(7)
P(1)–C(11)–C(12)	125(2)	P(3)–C(31)–C(32)	120(2)
P(1)–C(11)–C(15)	128(2)	P(3)–C(31)–C(35)	132(2)
P(2)–C(16)–C(15)	123(2)	P(4)–C(36)–C(35)	116(2)

[a] Numbers in parentheses are estimated standard deviations in the least significant digits.

(3–5 h), as determined by TLC analysis. Prolonged heating of the reaction solution led to complete consumption of cluster **2**, coupled with the gradual diminution of **3** and increase in cluster **4**. The two new clusters were isolated by column chromatography over silica gel and characterized in solution and by X-ray crystallography. Scheme 1 show the relationship between clusters **2**–**4**.

The IR spectrum for **3** in CH_2Cl_2 displayed two strong terminal ν(CO) bands at 2006 (s) and 1954 (vs) cm^{-1}, along with an intense semibridging CO group at 1912 cm^{-1}. The two ν(CO) bands of the anhydride moiety appear at 1789 and 1740 cm^{-1}. These two anhydride CO bands of cluster **3** are shifted ca. 30 cm^{-1} to lower energy in comparison to cluster **2** in concert with the coordination of the π bond of the bma ligand to an adjacent cobalt center and increased electron density to the anhydride moiety. The ^{31}P NMR spectrum of **3** recorded at 178 K revealed the presence of inequivalent ^{31}P groups at δ 25.30 and 29.57 consistent with the structure of **3** (vide infra). The broadness of both resonances is due to quadrupolar coupling to the ^{59}Co center and not an exchange process involving the bma ligand since the recorded chemical shifts were temperature invariant over from 298 to 178 K. The high-field shift exhibited by this type of P,P,π-chelated bma ligand is not unusual compared to analogous compounds prepared by our groups [24]. The ^{13}C NMR spectrum of a ^{13}CO enriched sample of $PhCCo_2Ni(CO)_3(\mu,\eta^2$-bma)Cp displayed three carbonyl resonances at δ 201.31, 209.46, and 223.79 in a 1:1:1 integral ratio at 223 K. The assignment for these CO groups is shown below, with the chemical shifts in keeping with accepted trends reported for other metal cluster compounds [25].

The P,P,π-coordination of the bma ligand to the cluster frame in **3** is readily seen in the ORTEP diagram of **3** that is shown in Fig. 3. The bma ligand functions as a 6e− donor ligand through chelation of the Co(1) center with the P(1) and P(2) centers and coordination of the Co(2) with the C(11)–C(15) π bond of the maleic anhydride moiety. The total valence electron count in $PhCCo_2Ni(CO)_3(\mu,\eta^2$-bma)Cp is unchanged relative to its precursor cluster **2** and the *nido* polyhedral core is maintained. The Ni–Co(1) [2.491(2) Å], Ni–Co(2) [2.420(2) Å], and Co(1)–Co(2) [2.405(1) Å] bond distances are in agreement with Ni–Co and Co–Co single-bond distances. The Ni–Co(2) bond best viewed as a donor–acceptor bond or a zwitterionic covalent bond when conventional electron formalism and the EAN rule are considered, as depicted below. The existence

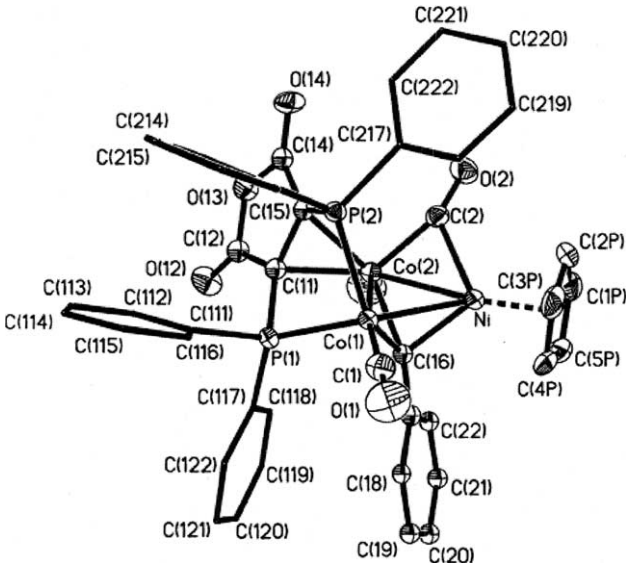

Fig. 3. ORTEP drawing of $PhCCo_2Ni(CO)_3(\mu,\eta^2\text{-bma})Cp$ (**3**) showing the thermal ellipsoids at the 50% probability level.

of a semibridging C(2)O(2) group that spans the Ni–Co(2) vector is confirmed by the Ni–C(2) and Co(2)–C(2) bond distances of 2.114(7) and 1.821(9) Å, respectively, and the bond angles of 128.0(7) and 156.3(7)° adopted by Ni–C(2)–O(2) and Co(2)–C(2)–O(2) linkages, respectively [26]. The adoption of a semibridging Ni–C(2)–O(2) interaction in **3** allows for unfavorable intramolecular contacts between this particular CO group and the phenyl group comprised of the C(217)–C(222) atoms to be eliminated. The bond distances found for the Co(2)–C(11) [2.025(9) Å], Co(2)–C(15) [2.064(8) Å], and C(11)–C(15) [1.43(1) Å] vectors are in good agreement with distances reported for other π-bound Co(alkene) compounds [27].

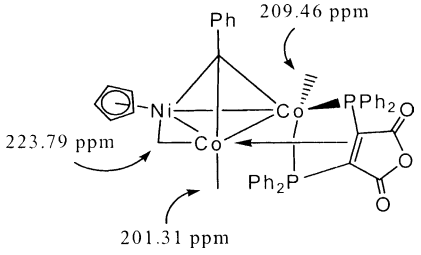

The observed ^{13}C NMR spectrum of cluster **4** was unexpected in that it contained four terminal carbonyl groups at δ 201.77, 206.10, 206.55, and 209.67 that integrate for one CO group each. The ^{31}P NMR spectrum of cluster **4** signaled the cleavage of a P–C bond in the bma ligand based on the two ^{31}P chemical shifts at δ 63.88 and 170.94 at 178 K. The lower field resonance is ascribed to a bridging phosphido moiety [28], with the assignment of the remaining resonance still equivocal at this point. Examination of cluster **4** from 289–178 K revealed that the linewidth of the high-field resonance remained sharp over all temperatures, ruling out a Co-bound phosphine moiety but not that of phosphine attack on the benzylidyne cap or the nickel center. Since precedents for both of these latter modes of ligand attack have been found in this genre of cluster by us [6], the nature of the bma-derived fragment and its coordination to the metallic frame in **4** were resolved by X-ray analysis.

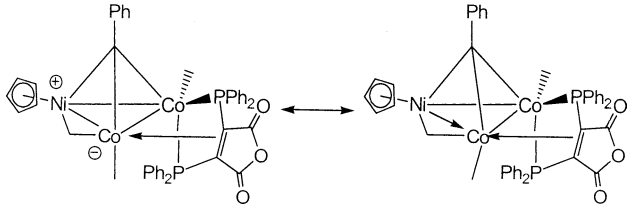

The ORTEP diagram of **4** is shown in Fig. 4, where the presence of a phosphido moiety and an opening of the triangular metal frame constitute the prominent structural features in this 50-valence electron cluster. The structure adopted by $Co_2Ni(CO)_4Cp[\mu_2,\eta^2,\eta^1\text{-}C(Ph)C{=}C(PPh_2)C(O)OC(O)](\mu_2\text{-}PPh_2)$ is readily understood through application of Polyhedral Skeletal Electron Pair (PSEP) theory. Here, the product cluster **4** may by viewed as a four-vertex *hypho* cluster that possesses 8 SEP and whose polyhedral shape may be traced back to the parent four-vertex *nido* cluster **3** before the formal association of two additional SEP. The observed Ni–Co(1) [2.434(2) Å] and Co(1)–Co(2) [2.595(2) Å] bond distances are unremarkable when compared to other structurally characterized Ni- and Co-containing polynuclear complexes. The Ni···Co(2) distance of 3.825(2) Å clearly precludes any bonding interactions between these two metal centers. The μ_2,η^2,η^1-C(Ph)C=C(PPh_2)C(O)OC(O) ligand functions as a 6e− donor ligand and is attached

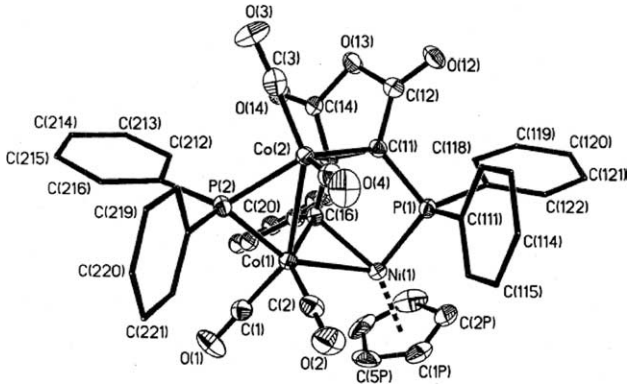

Fig. 4. ORTEP drawing of $Co_2Ni(CO)_4Cp[\mu_2,\eta^2,\eta^1\text{-}C(Ph)C{=}C(PPh_2)C(O)OC(O)](\mu_2\text{-}PPh_2)$ (**4**) showing the thermal ellipsoids at the 50% probability level. The solvent molecule has been omitted for clarity.

to the all three metal atoms in a fashion analogous to that found by us in the tricobalt cluster $Co_3(CO)_6[\mu_2,\eta^2,\eta^1$-C(R)C=C($PPh_2$)C(O)OC(O)]($\mu_2$-$PPh_2$). [4] The structure of **4** unequivocally establishes the attack of the PPh_2 moiety in this 6e− ligand to the CpNi center, a fact fully consistent with the temperature invariant high-field ^{31}P resonance. The Co(1)–P(2) and Co(2)–P(2) distances of 2.164(3) and 2.167(3) Å, respectively, and the Co(1)–P(2)–Co(2) bond angle of 73.61(9)° agree well with other structurally characterized cobalt-bound phosphido groups [29]. The torsion angle of ca. 20° for the P(2)–Ni–Co(1)–Co(2) linkage reveals the nearly planar orientation of these four atoms. The bonding of the maleic anhydride C(11)–C(15) π bond to the Co(2) center and the four terminal CO groups are unexceptional and require no comment.

We next sought to establish the relationship between $PhCCo_2Ni(CO)_3(\mu,\eta^2$-bma)Cp and $Co_2Ni(CO)_4Cp[\mu_2,\eta^2,\eta^1$-C(Ph)C=C($PPh_2$)C(O)OC(O)]($\mu_2$-$PPh_2$). Independent thermolysis reactions employing isolated samples of cluster **3** did indeed afford cluster **4** when the reaction was monitored by IR and TLC analyses and fully validated the reaction pathway shown in Scheme 1. The kinetics for the conversion of $PhCCo_2Ni(CO)_4(\eta^2$-bma)Cp to $PhCCo_2Ni(CO)_3(\mu,\eta^2$-bma)Cp were also investigated to determine whether a dissociative CO loss mechanism or an associative attack of the maleic anhydride π bond, coupled with CO loss, was responsible for the formation of cluster **3**. These reactions were studied by IR spectroscopy in toluene solution over the temperature range of 92–107 °C by following the change in concentration in antisymmetric ν(CO) band of the anhydride moiety at 1765 cm^{-1}. All reactions followed first-order kinetics for at least three half-lifes, as verified from linear plots of ln A_t vs time. The slopes of such plots afforded the first-order rate constants given in Table 4. The effect of added CO on the reaction was explored (entry 5), where it is found that the rate of the reaction is retarded by ca. a factor of 10 with respect to the reaction run under argon. The calculated activation parameters for **2** → **3** ($\Delta H^{\neq}$ = 34.8 ± 0.9 kcal/mol and $\Delta S^{\neq}$ = 18 ± 3 eu) and the observed CO inhibition support a unimolecular process involving a dissociative CO loss as the rate-limiting step and that obeys the general rate law [30,31]:

$$\text{rate} = k_1k_2[PhCCo_2Ni(CO)_4(\eta^2\text{-bma})Cp]/k_{-1}[CO] + k_2$$

The stoichiometry in going from **3** to **4** mandates the capture of an extra CO ligand as cluster **4** possesses one additional CO group relative to $PhCCo_2Ni(CO)_3(\mu,\eta^2$-bma)Cp. Provided that cluster **3** serves as a precursor to cluster **4** and functions as the source of CO to the same, the amount of product that can be formed in any thermolysis reaction is limited to no more than 75%. These aspects pertaining to the role of $PhCCo_2Ni(CO)_3(\mu,\eta^2$-bma)Cp were tested by an independent thermolysis reaction employing pure **3**. Refluxing a known amount of cluster **3** in DCE for ca. 5 h led to the near complete consumption of **3** and the production of cluster **4** as the major product by TLC analysis, along with a noticeable amount of material that remained at the origin of the TLC plate. Cluster **4** was subsequently isolated by chromatography in ca. 50% of its theoretical yield.

Table 4
Experimental rate constants for the transformation of $PhCCo_2Ni(CO)_4(\eta^2$-bma)Cp (**2**) to $PhCCo_2Ni(CO)_3(\mu,\eta^2$-bma)Cp (**3**)[a]

Entry no.	T (°C)	$10^5\ k_{obsd}$ (s^{-1})
1	92.3	9.74 ± 0.70
2	97.3	16.5 ± 1.1
3	102.3	33.1 ± 4.0
4	106.6	58.7 ± 2.9
5[b]	106.6	5.82 ± 0.18

[a] From ca. 5.50×10^{-3} M $PhCCo_2Ni(CO)_4(\eta^2$-bma)Cp in toluene solvent by following the decrease in the ν(CO) band at 1765 cm^{-1}. All kinetic data represent the average of two, independent measurements.
[b] Reaction conducted in the presence of 1 atm of CO.

3.3. Thermolysis of $Co_2Ni(CO)_4Cp[\mu_2,\eta^2,\eta^1$-C(Ph)C=C($PPh_2$)C(O)OC(O)]($\mu_2$-$PPh_2$) and decomposition to the mononuclear complex CpNi[PPh_2CPhC=C(PPh_2)C(O)OC(O)]

Prolonged thermolysis of the phosphido-bridged cluster $Co_2Ni(CO)_4Cp[\mu_2,\eta^2,\eta^1$-C(Ph)C=C($PPh_2$)C(O)OC(O)]($\mu_2$-$PPh_2$) (**4**) in refluxing DCE yields the mononuclear compound CpNi[PPh_2CPhC=C(PPh_2)C(O)OC(O)] (**5**) as the final degradation product in the reaction between $PhCCo_2Ni(CO)_6Cp$ (**1**) and bma. Compound **5** was isolated in low yield due to the extensive decomposition that accompanies the thermolysis of **4**. A Cp resonance at δ 4.92 in the ^{1}H NMR spectrum of **5** confirmed the existence of a CpNi group, while the observation of two ν(CO) bands at 1746 and 1714 cm^{-1} supported the presence of an anhydride moiety in the isolated material. The two sharp ^{31}P doublets found at δ 12.22 and 42.07 in the ^{31}P NMR spectrum ruled out the presence of cobalt-bound phosphine or phosphido groups. The identity of compound **5** was established by X-ray diffraction analysis. The molecular structure of **5**, as shown in Fig. 5, consists of two independent molecules of **5** that may be viewed as originating from the formal insertion of the carbyne fragment ''PhC'' into one of the P–C bonds of the mononuclear compound CpNi(bma). Both molecules of CpNi[PPh_2CPhC=C(PPh_2)C(O)OC(O)] consist of a six-membered ring, where the pairwise equivalent Ni(1)–P(1) and Ni(2)–P(3) bonds reveal a mean distance of 2.150 Å and the Ni(1)–P(2) and Ni(2)–P(4) bonds exhibit an average bond length of 2.149 Å. The phosphorus–ylide P(2)–C(16) and P(4)–C(36) bond distances closely match the distances found for the P(1)–C(11) and P(3)–C(31) vectors, where a mean

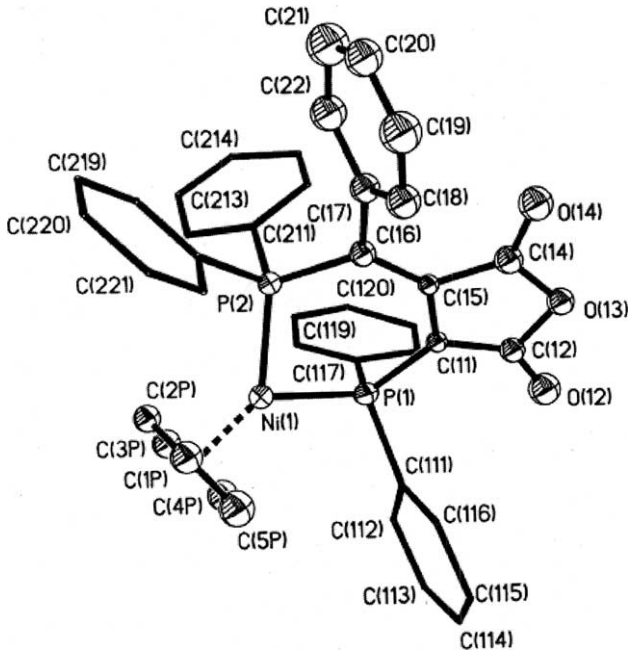

Fig. 5. ORTEP drawing of one of the two molecules of $CpNi[PPh_2CPhC{=}C(PPh_2)C(O)OC(O)]$ (**5**) in the unit cell showing the thermal ellipsoids at the 50% probability level.

bond distance of 1.78 Å is found for all four bonds. The similarity found in these distances suggests that these four phosphorus–carbon bonds possess significant single-bond character. The maleic anhydride carbon–carbon π bond in each molecule of **5** [C(11)–C(15) 1.45(3) Å; C(31)–C(36) 1.38 Å] is lengthened slightly with respect to a simple alkene linkage but is in excellent agreement to the analogous distance found in the X-ray structure of $CpNi[Ph_2PC{=}C(C_5H_6PPh_2)C(O)OC(O)]$, which has been obtained from the reaction between nickelocene and bma [32]. The dihedral angle of ca. 60° found between the planes comprised by the maleic anhydride moiety and the cyclopentadienyl carbon atoms in both molecules of **5** confirms that these moieties do not adopt an orthogonal orientation. The remaining bond distances and angles are unexceptional and require no comment.

4. Conclusions

The reaction between the heterometallic cluster $PhCCo_2Ni(CO)_6Cp$ (**1**) and 2,3-bis(diphenylphosphino)maleic anhydride has been studied and found to give initially the diphosphine-substituted cluster $PhCCo_2Ni(CO)_4(\eta^2\text{-bma})Cp$ (**2**), where the bma ligand tethers the two cobalt centers. VT IR and ^{31}P NMR measurements have revealed that the bma ligand is fluxional in solution and is in equilibrium with the cobalt-chelated isomer. Heating cluster **2** leads to a rate-limiting loss of CO, followed by a rapid coordination of the maleic anhydride π bond and formation of $PhCCo_2Ni(CO)_3(\mu,\eta^2\text{-bma})Cp$ (**3**). Thermolysis of **3** furnishes the 8 SEP cluster $Co_2Ni(CO)_4Cp[\mu_2,\eta^2,\eta^1\text{-}C(Ph)C{=}C(PPh_2)C(O)OC(O)](\mu_2\text{-}PPh_2)$ (**4**), which in turn gives the mononuclear complex $CpNi[PPh_2CPhC{=}C(PPh_2)C(O)OC(O)]$ (**5**) as the final product of the thermolysis reaction. The isolation and structural characterization of compounds **2**–**5** have allowed us to study and chart each step of the thermal degradation of the original bma-substituted cluster **2**.

5. Supporting information available

Crystallographic data for the structural analyses have been deposited with the Cambridge Crystallographic Data Center, CCDC No. 244754 for **2**; 244755 for **3**; 244756 for **4**; and 245326 for **5**. Copies of this information may be obtained free of charge from the Director, CCDC, 12 Union Road, Cambridge, CB2 1EZ UK [fax: +44(1223)336-033; e-mail: deposit@ccdc.ac.uk or http://www:ccdc.cam.ac.uk].

Acknowledgment

Financial support from the Robert A. Welch Foundation (B-1093-M.G.R.) is greatly appreciated.

References

[1] (a) P.A. Dawson, B.H. Robinson, J. Simpson, J. Chem. Soc., Dalton Trans. (1979) 1762;
(b) K. Hinkelmann, J. Heinze, H.-T. Schacht, J.S. Field, H. Vahrenkamp, J. Am. Chem. Soc. 111 (1989) 5078;
(c) G.J. Bezems, P.H. Rieger, S. Visco, J. Chem. Soc., Chem. Commun. (1981) 265;
(d) A.L. Downard, B.H. Robinson, J. Simpson, Organometallics 5 (1986) 1132–1140;
(e) S.B. Colbran, B.H. Robinson, J. Simpson, Organometallics 2 (1983) 952;
(f) T.W. Matheson, B.H. Robinson, W.S. Tham, J. Chem. Soc. A (1971) 1457.
[2] (a) M.F. D'Agostino, C.S. Frampton, M.J. McGlinchey, Organometallics 10 (1991) 1383;
(b) Y. Takahashi, M. Akita, Y. Moro-oka, Chem. Commun. (1997) 1557;
(c) J.T. Mague, S.E. Dessens, J. Organomet. Chem. 262 (1984) 347.
[3] (a) G. Balavoine, J. Collin, J.-J. Bonnet, G. Lavigne, J. Organomet. Chem. 280 (1985) 429;
(b) A.J. Downard, B.H. Robinson, J. Simpson, Organometallics 5 (1986) 1122;
(c) M.-J. Don, M.G. Richmond, W.H. Watson, R.P. Kashyap, Acta Crystallogr. 47C (1991) 20;
(d) S. Onaka, A. Mizuno, S. Takagi, Chem. Lett. (1989) 2037;
(e) S. Onaka, T. Moriya, S. Takagi, A. Mizuno, H. Furuta, Bull. Chem. Soc. Jpn. 65 (1991) 1415;
(f) A.J. Downard, B.H. Robinson, J. Simpson, J. Organomet. Chem. 447 (1993) 281;

(g) G.A. Acum, M.J. Mays, P.R. Raithby, H.R. Powell, G.A. Solan, J. Chem. Soc., Dalton Trans. (1997) 3427;
(h) M.-J. Don, M.G. Richmond, W.H. Watson, M. Krawiec, R.P. Kashyap, J. Organomet. Chem. 418 (1991) 231;
(i) W.H. Watson, A. Nagl, S. Hwang, M.G. Richmond, J. Organomet. Chem. 445 (1993) 163;
(j) K. Yang, S.G. Bott, M.G. Richmond, J. Organomet. Chem. 454 (1993) 273;
(k) G.A. Acum, M.J. Mays, P.R. Raithby, G.A. Solan, J. Organomet. Chem. 508 (1996) 137;
(l) S.G. Bott, J.C. Wang, M.G. Richmond, J. Chem. Crystallogr. 28 (1998) 401;
(m) S. Aime, M. Botta, R. Gobetto, D. Osella, J. Organomet. Chem. 320 (1987) 229.

[4] (a) K. Yang, J.M. Smith, S.G. Bott, M.G. Richmond, Organometallics 12 (1993) 4779;
(b) H. Shen, S.G. Bott, M.G. Richmond, Inorg. Chim. Acta 250 (1996) 195.

[5] The reactivity study of the hydrogen- and formyl-capped clusters with bma and the related ligand bpcd has recently been completed. W.H. Watson, J. Liu, M.G. Richmond, unpublished results.

[6] S.G. Bott, K. Yang, K.A. Talafuse, M.G. Richmond, Organometallics 22 (2003) 1383.

[7] (a) D. Fenske, H. Becher, Chem. Ber. 107 (1974) 117;
(b) D. Fenske, Chem. Ber. 112 (1979) 363.

[8] M.O. Nestle, J.E. Hallgren, D. Seyferth, Inorg. Synth. 20 (1980) 226.

[9] R.B. King Organometallic Syntheses, vol. 1, Academic Press, New York, 1965.

[10] (a) H. Beurich, R. Blumhofer, H. Vahrenkamp, Chem. Ber. 115 (1982) 2409;
(b) R. Blumhofer, K. Fischer, H. Vahrenkamp, Chem. Ber. 119 (1986) 194.

[11] D.F. Shriver, The Manipulation of Air-sensitive Compounds, McGraw-Hill, New York, 1969.

[12] A.J. Gordon, R.A. Ford, The Chemist's Companion. A Handbook of Practical Data Techniques and References, Wiley, New York, 1976.

[13] (a) For differentiation of bridging versus chelating diphosphine compounds through ^{31}P NMR spectroscopy, see: P.E. Garrou, Chem. Rev. 81 (1981) 229;
(b) M.R. Churchill, R.A. Lashewycz, J.R. Shapley, S.I. Richter, Inorg. Chem. 19 (1980) 1277;
(c) M.G. Richmond, J.K. Kochi, Organometallics 6 (1987) 245.

[14] (a) For the effect of scalar coupling on a cobalt-bound phosphorus center, see: M. Schwartz, M.G. Richmond, A.F.T. Chen, G.E. Martin, J.K. Kochi, Inorg. Chem. 27 (1988) 4698;
(b) M.-J. Don, M.G. Richmond, Inorg. Chem. 30 (1991) 1703.

[15] (a) W.G. Dauben, W.W. Epstein, J. Org. Chem. 24 (1959) 1595;
(b) N.B. Colthup, Appl. Spectr. 39 (1985) 1030.

[16] In theory both the symmetric and antisymmetric carbonyl stretching bands of the anhydride moiety in the isomers of cluster **2** could be used in the band-area measurements. However, the area under the antisymmetric stretch of each isomer exhibited poor linear behavior over the temperature range investigated and was not utilized in the van't Hoff treatment of the IR data. Moreover, analysis of the area under the two antisymmetric anhydride bands at 173 K afforded a bridging:chelating ratio of 66:34 in poor agreement with the ratio determined by ^{31}P NMR spectroscopy. The use of the symmetric CO band to quantify the isomeric composition was strengthened by a calculated bridging:chelating ratio at 173 K that was identical with the ^{31}P NMR data.

[17] (a) K.A. Sutin, J.W. Kolis, M. Mlekuz, P. Bougeard, B.G. Sayer, M.A. Quilliam, R. Faggiani, C.J.L. Lock, M.J. McGlinchey, G. Jaouen, Organometallics 6 (1987) 439;
(b) M.F. D'Agostino, M.J. McGlinchey, Polyhedron 7 (1988) 807.

[18] (a) For some examples of intramolecular phosphine exchange reactions in other polynuclear systems, see: A.M. Bradford, G. Douglas, L. Manojlovic-Muir, K.W. Muir, R.J. Puddephatt, Organometallics 9 (1990) 409;
(b) R.D. Adams, B. Captain, W. Fu, P.J. Pellechia, Chem. Commun. (2000) 937;
(c) E. Gullo, S. Detti, G. Laurenczy, R. Roulet, J. Chem. Soc., Dalton Trans. (2002) 4577;
(d) G. Laurenczy, G. Bondietti, R. Ros, R. Roulet, Inorg. Chim. Acta 247 (1996) 65.

[19] (a) The possibility of bma fluxionality in cluster **2** arising from a CO loss, ligand rearrangement, CO capture scheme can be eliminated from consideration based on the extrapolated rate constant for dissociative CO loss of ca. $10^{-9}\,s^{-1}$ at 273 K.;
(b) cf.: the extrapolated value for dissociative CO loss of ca. $3\times10^{-7}\,s^{-1}$ in $PhCCo_3(CO)_9$ at 273 K.A. Cartner, R.G. Cunninghame, B.H. Robinson, J. Organomet. Chem. 92 (1975) 49.

[20] D.M.P. Mingos, D.J. Wales, Introduction to Cluster Chemistry, Prentice-Hall, Englewood Cliffs, NJ, 1990.

[21] For the structural details on $PhCCo_2Ni(CO)_4$ [(Z)-$Ph_2PCH{=}CHPPh_2$]Cp, see: S.G. Bott, K. Yang, S.-H. Huang, M.G. Richmond, J. Chem. Crystallogr. 34 (2004) 885.

[22] (a) R. Blumhofer, K. Fischer, H. Vahrenkamp, Chem. Ber. 119 (1986) 194;
(b) L.R. Byers, V.A. Uchtman, L.F. Dahl, J. Am. Chem. Soc. 103 (1981) 1942;
(c) J.J. Maj, A.D. Rae, L.F. Dahl, J. Am. Chem. Soc. 104 (1982) 3054;
(d) H. Beurich, H. Vahrenkamp, Angew. Chem., Int. Ed. Engl. 17 (1978) 863.

[23] R.C. Weast (Ed.), Handbook of Chemistry and Physics, 56th ed., CRC Press, Cleveland, OH, 1975.

[24] (a) H. Shen, S.G. Bott, M.G. Richmond, Organometallics 14 (1995) 4625;
(b) K. Yang, J.A. Martin, S.G. Bott, M.G. Richmond, Organometallics 15 (1996) 2227;
(c) S.G. Bott, K. Yang, J.C. Wang, M.G. Richmond, Inorg. Chem. 39 (2000) 6051.

[25] (a) M.G. Richmond, J.K. Kochi, Inorg. Chem. 25 (1986) 1334;
(b) S. Aime, L. Milone, R. Rossetti, P.L. Stanghellini, Inorg. Chim. Acta 25 (1977) 103;
(c) D.J. Darensbourg, B.S. Peterson, R.E. Schmidt Jr., Organometallics 1 (1982) 306.

[26] C.P. Horwitz, D.F. Shriver, Adv. Organomet. Chem. 23 (1984) 219.

[27] A.G. Orpen, L. Brammer, F.H. Allen, O. Kennard, D.G. Watson, R. Taylor, J. Chem. Soc., Dalton Trans. (1989) S1.

[28] A.J. Carty, S.A. MacLaughlin, D. Nucciarone, in: J.G. Verkade, L.D. Quin (Eds.), Phosphorus-31 NMR Spectroscopy in Stereochemical Analysis, VCH Publishers, Deerfield Beach, FL, 1987 (Chapter 16).

[29] (a) T.A. Albright, S.-K. Kang, A.M. Arif, A.J. Bard, R.A. Jones, J.K. Leland, S.T. Schwab, Inorg. Chem. 27 (1988) 1246;
(b) A.D. Harley, R.R. Whittle, G.L. Geoffroy, Organometallics 2 (1983) 60;
(c) R. Regragui, P.H. Dixneuf, N.J. Taylor, A.J. Carty, Organometallics 3 (1984) 1020;
(d) S. Onaka, H. Muto, Y. Katsukawa, S. Takagi, J. Organomet. Chem. 543 (1997) 241.

[30] (a) J.D. Atwood, Inorganic and organometallic reaction mechanisms, Brooks/Cole Publisher Co., Monterey, CA, 1985;
(b) R.B. Jordan, Reaction Mechanisms of Inorganic and Organometallic Systems, second ed., Oxford University Press, New York, 1998.

[31] The rigorous rate law in the absence of added CO ($k_2 > k_{-1}$[CO]) reduces to simple first-order expression: rate = k_1[$PhCCo_2Ni(CO)_4(\eta^2$-bma)Cp].

[32] W. Bensmann, D. Fenske, Angew. Chem., Int. Ed. Engl. 17 (1978) 462.